Figures and figure supplements

Prdm1 positively regulates liver Group 1 ILCs cancer immune surveillance and preserves functional heterogeneity

Jitian He, Le Gao and Peiying Wang *et al*.

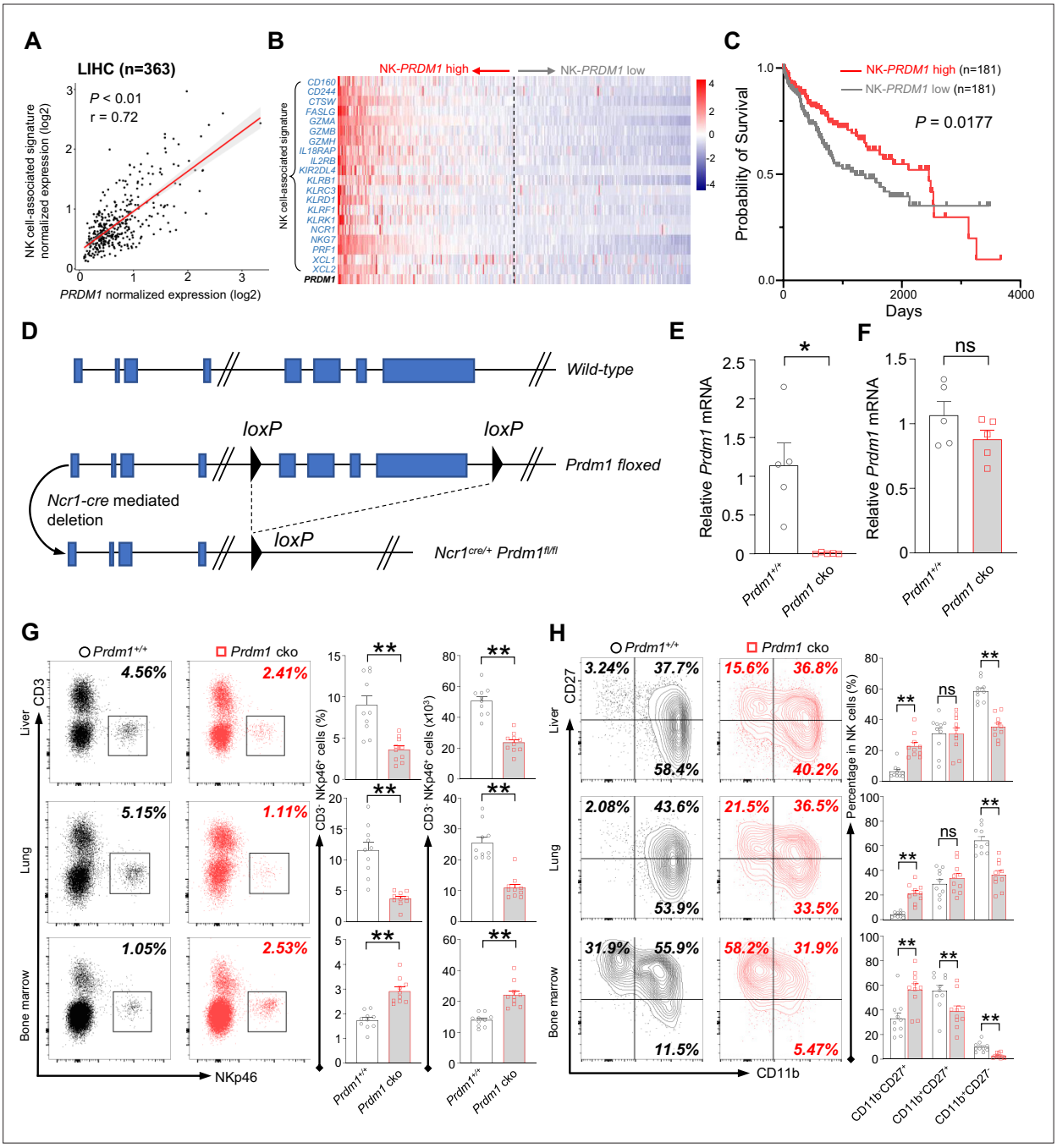

Figure 1. *Prdm1* promotes NK cell homeostasis and terminal maturation. (**A**) Correlation between the average expression of NK cell-associated signature and *PRDM1* in LIHC (Liver Hepatocellular Carcinoma; n=363) patients sourced from TCGA datasets. (**B**) Heatmap of the ordered, z-score normalized expression values for *PRDM1* and NK cell-associated genes in liver cancer patients. High and low expression of *NK-PRDM1* signature are indicated. (**C**) Prognostic value of the *NK-PRDM1* signature for overall survival of liver cancer patients comparing high and low samples with a median cutoff. (**D**) Schematic representation of the Prdm1-conditional knockout mouse model. Targeted exon 6–8 of *Prdm1* (top) is flanked with *loxP* sites (middle). Ncr1-expressed Cre recombinase was used to generate the *Prdm1* cko allele (bottom). (**E and F**) Real-time RT-PCR quantification of *Prdm1* expression in NKp46$^+$ cells (**E**) and splenocytes (**F**) to determine the presence of *Prdm1* (n=5). (**G**) Representative flow cytometric plots (left) and quantification (right) of the proportion and absolute number of CD45$^+$CD3$^-$NKp46$^+$ cells among lymphocytes in liver, lung, and bone marrow (n=10). (**H**) Representative flow cytometric plots (left) of the CD11b and CD27 expression within CD3$^-$NK1.1$^+$NKp46$^+$CD49b$^+$ cells in liver, lung, and bone marrow (n=10). Right panel showed the percentage of distinct maturation stages of NK cells. Data are presented as the mean ± SEM and were analyzed by two-tailed, paired t-test. Differences were evaluated between littermates. Each circle and square on graphs represents an individual mouse; *P*, p-value; r, pearson correlation coefficient; *, p<0.05; **, p<0.01, ns, not significant.

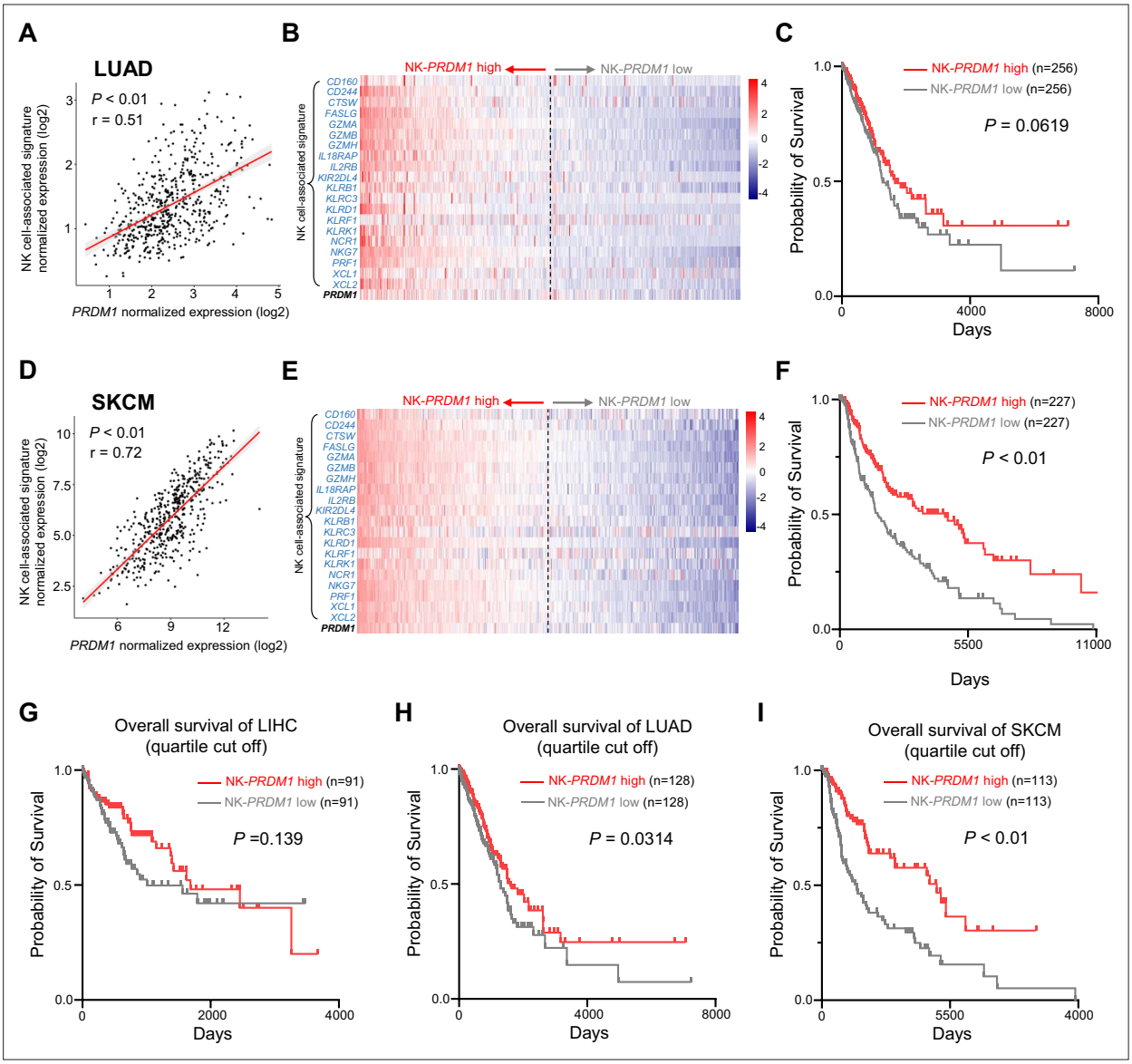

Figure 1—figure supplement 1. High expression of *PRDM1-NK* signature predicts better overall survival of cancer patients. (**A and D**) Correlation between the average expression of NK cell-associated signature and *PRDM1* in lung adenocarcinoma (**A**) (LUAD, n=497) and skin cutaneous melanoma (SKCM, n=454) (**D**) patients from TCGA datasets. (**B and E**) Heatmap of the ordered, z-score normalized expression values for *PRDM1* and NK cell-associated genes in LUAD (**B**) and SKCM (**E**) patients. High and low expression of *NK-PRDM1* signature are indicated. (**C and F**) Prognostic value of the *NK-PRDM1* signature for overall survival of LUAD (**C**) and SKCM (**F**) patients comparing high and low samples with a median cutoff. (**G–I**) Prognostic value of the *NK-PRDM1* signature for overall survival of LIHC (**G**), LUAD (**H**), and SKCM (**I**) patients comparing high and low samples with a quartile cutoff. *P*, p-value; r, pearson correlation coefficient.

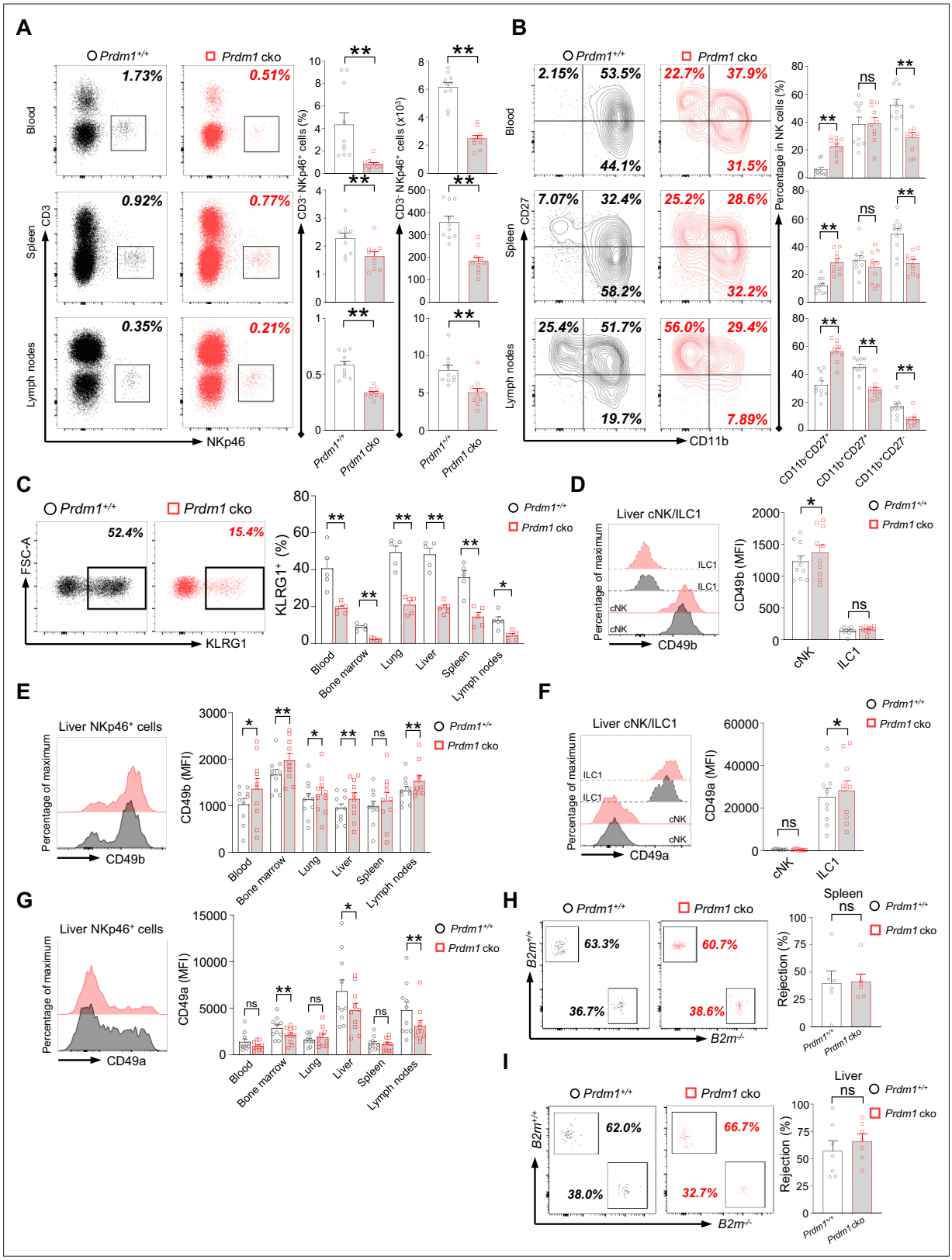

Figure 1—figure supplement 2. *Prdm1* plays an essential role in group 1 ILCs homeostasis and maturation. (**A**) Representative flow cytometric plots (left) and quantification (right) of the proportion and absolute number of CD45$^+$CD3$^-$NKp46$^+$ cells among lymphocytes in liver, lung, and bone marrow (n=10). (**B**) Representative flow cytometric plots (left) of the CD11b and CD27 expression within CD3$^-$NK1.1$^+$NKp46$^+$CD49b$^+$ cells in liver, lung, and bone marrow (n=10). Right panel showed the percentage of distinct maturation stages of NK cells. (**C**) Representative flow cytometry analyses of

Figure 1—figure supplement 2 continued on next page

Figure 1—figure supplement 2 continued

KLRG1^{+} cells in CD3^{-}NK1.1^{+}NKp46^{+}CD49b^{+} cells in liver, and their quantification in blood, bone marrow, lung, liver, spleen, and lymph nodes (n=5). (**D–G**) Representative flow cytometry plots of the mean fluorescence intensities (MFIs) of CD49b and CD49a in liver cNK cells and ILC1s (**D and F**), and in NKp46^{+} cells in blood, bone marrow, lung, liver, spleen, and lymph nodes (n=10) (**E and G**). (**H and I**) Splenocytes from *B2m*$^{-/-}$ and *B2m*$^{+/+}$ were labeled with CFDASE and eF670, respectively. Labeled cells were 1:1 mixed and injected i.v. into *Prdm1*$^{+/+}$ and *Prdm1* cko recipient mice to evaluate in vivo NK cell target-killing ability. Representative flow cytometric plots (left) of transferred cells recovered from recipient mice and percentage (right) of NK-cell-specific rejection of donor cells in spleen (n=6) (**H**) and liver (n=7) (**I**) between *Prdm1*$^{+/+}$ and *Prdm1* cko mice. Data are presented as the mean ± SEM and were analyzed by two-tailed, paired t-test. Differences were evaluated between littermates. Each circle and square on graphs represents an individual mouse; *P*, p-value; *, p<0.05; **, p<0.01, ns, not significant.

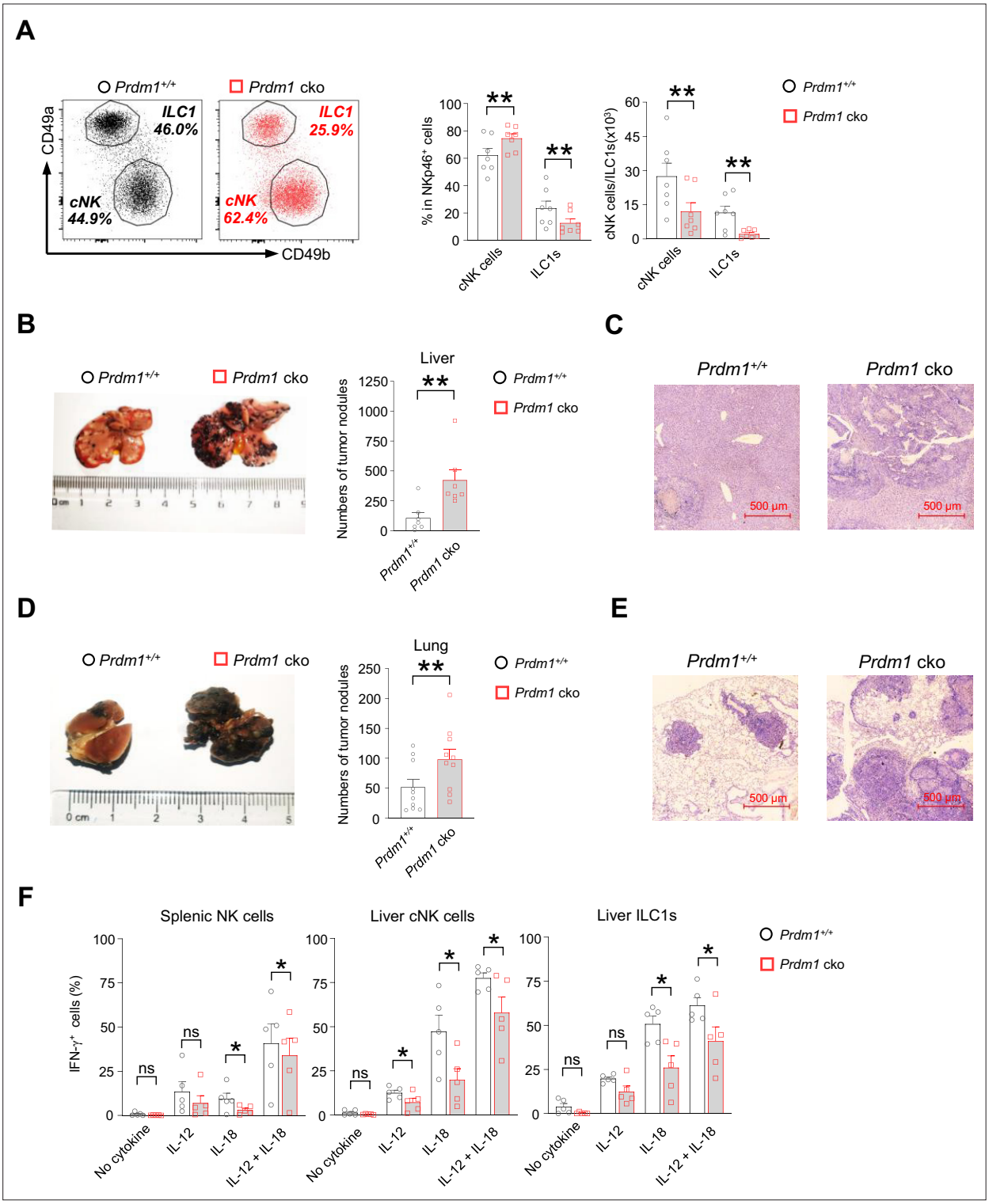

Figure 2. *Prdm1* is required for group 1 ILCs to control tumor metastasis. (**A**) Representative flow cytometric plots (left) of liver cNK cells ($CD49a^-CD49b^+$) and ILC1s ($CD49a^+CD49b^-$) from *Prdm1*$^{+/+}$ and *Prdm1* cko mice. The two bar graphs (right) quantitate the percentages and absolute numbers of cells respectively (n=7). (**B and D**) Representative image (left) and quantification (right) of tumor nodes on the livers (n=7) (**B**) and lungs (n=10) (**D**) of *Prdm1*$^{+/+}$ and *Prdm1* cko mice at day 14 or 21 after inoculation with B16F10 melanoma cells. (**C and E**) Representative histopathological images of liver (**C**) and lung (**E**) tissues stained by hematoxylin-eosin to detect tumor metastasis. Red bar indicates 500 μm distance under the microscope. (**F**) Liver cells and splenocytes were co-stimulated in the presence or absence of IL-12 and IL-18 for 12 hr. GolgiStop was added 4 hr before intracellular staining of IFN-γ. The graphs showed percentage of IFN-γ^+ splenic cNK cells, liver cNK cells and ILC1s from *Prdm1*$^{+/+}$ and *Prdm1* cko mice (n=5). Data are

Figure 2 continued on next page

Figure 2 continued

presented as the mean ± SEM and were analyzed by two-tailed, paired t-test. Differences were evaluated between littermates. Each circle and square on graphs represents an individual mouse; *P*, p-value; *, p<0.05; **, p<0.01, ns, not significant.

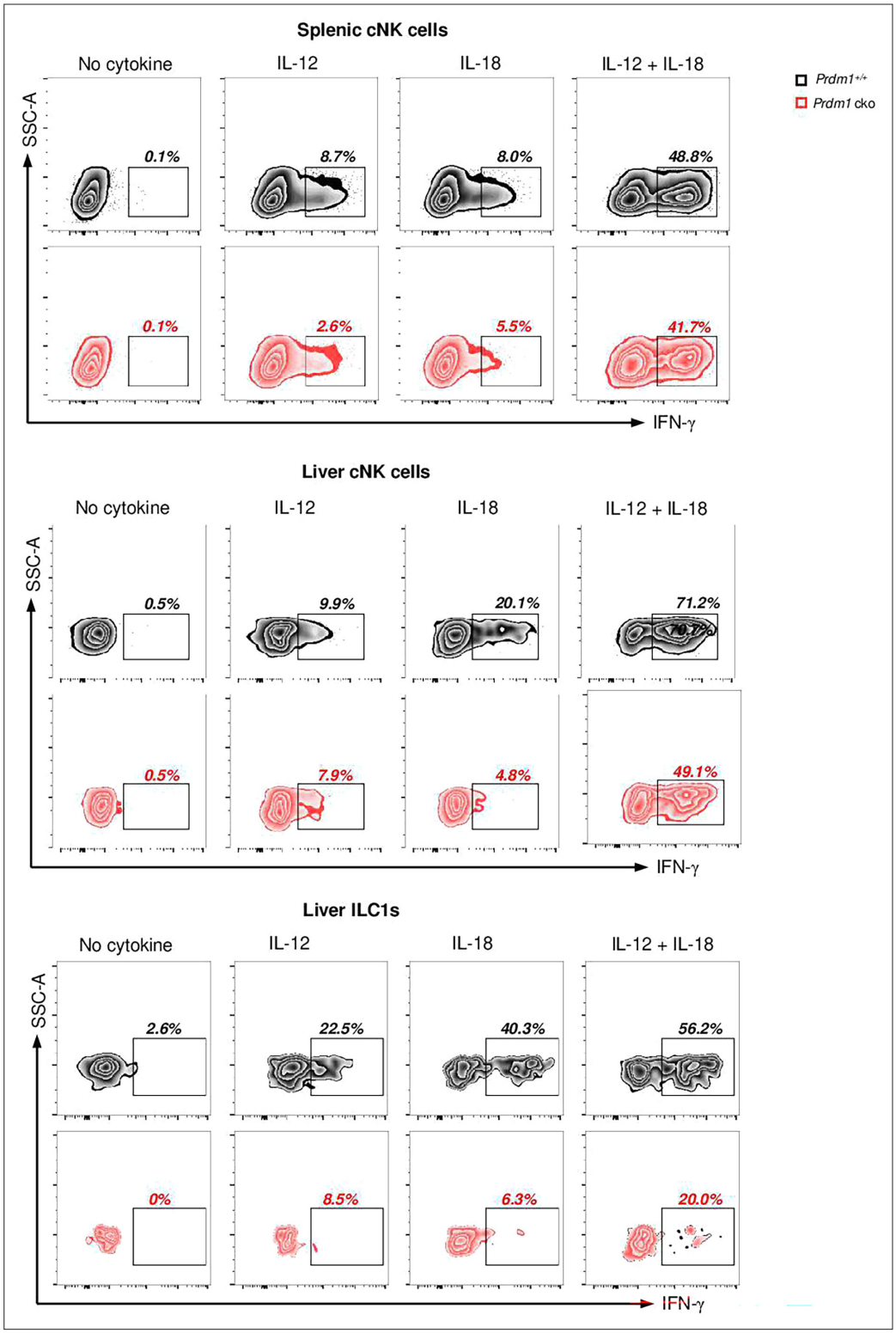

Figure 2—figure supplement 1. *Prdm1* affects the IFN-γ secretion ability of type I ILCs. Representative flow cytometric plot showing the frequency of IFN-γ$^+$ cNK cells and ILC1s in spleen and liver between *Prdm1*$^{+/+}$ and *Prdm1* cko mice (n=5). Liver cells and splenocytes were costimulated in the presence or absence of IL-12 and IL-18 for 12 hr. GolgiStop was added 4 hr before intracellular staining of IFN-γ. Data are presented as the mean ± SEM and were analyzed by two-tailed, paired t-test. Differences were evaluated between littermates. Each circle and square on graphs represents an individual mouse; *P*, p-value; *, p<0.05; **, p<0.01, ns, not significant.

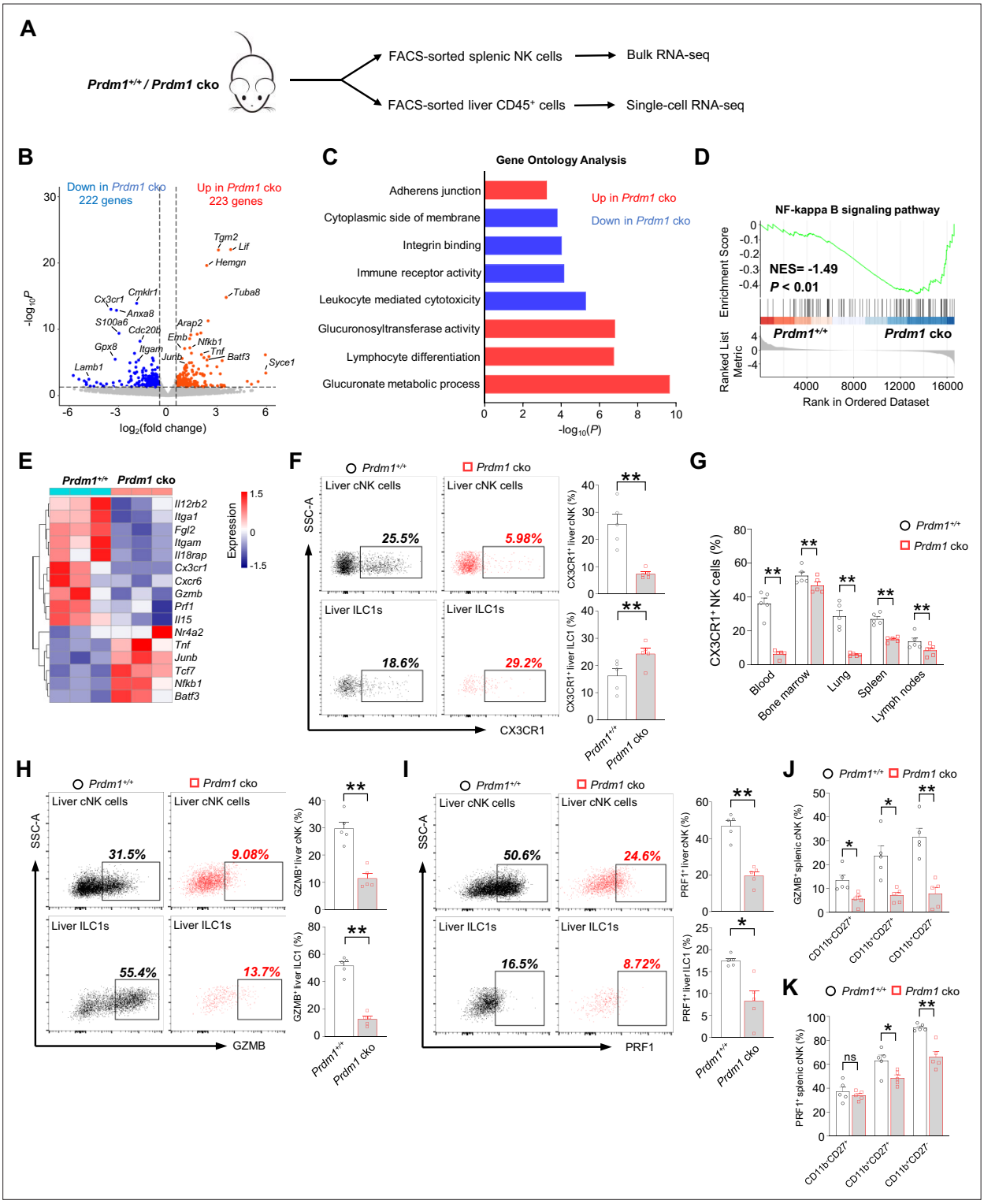

Figure 3. Bulk RNA-seq reveals Prdm1-mediated functions in splenic cNK cells. (**A**) Splenic cNK cells and liver CD45$^+$ cells were sorted from *Prdm1*$^{+/+}$ and *Prdm1* cko mice using flow cytometry, and prepared for bulk RNA-seq and single-cell RNA-seq analysis. (**B**) Volcano plot of the bulk RNA-seq differentially expressed genes (DEGs) (log_2|fold change|>0.5; p<0.05) in splenic cNK cells between *Prdm1*$^{+/+}$ and *Prdm1* cko mice. Upregulated and downregulated genes in *Prdm1* cko cells were highlighted in red and blue. (**C**) Enriched Gene Ontology (GO) terms of DEGs in *Prdm1* cko cells compared *Prdm1*$^{+/+}$ cells. The Enrichment gene set in upregulated (red) and downregulated (blue) genes were indicated in different colour. Bar length represents statistical significance. (**D**) Gene Set Enrichment Analysis (GSEA) showing the enrichment of NF-kappa B signaling pathway of DEGs in *Prdm1* cko cells compared *Prdm1*$^{+/+}$ cells. NES, normalized enrichment score. (**E**) Heatmap of selected genes from DEGs. Shown is z-score transformed

Figure 3 continued on next page

Figure 3 continued

expression of DEGs. (**F**) Representative flow cytometric plots (left) and cumulative data (right) of the percentage and absolute numbers of CX3CR1$^+$ cells in liver cNK cells and ILC1s (n=5). (**G**) Quantification of CX3CR1$^+$ cells in NK cells in blood, bone marrow, lung, liver, spleen, and lymph nodes (n=5). (**H and I**) Representative flow cytometric plots (left) and cumulative data (right) showing the proportion of GZMB$^+$ (**H**) and PRF1$^+$ (**J**) liver cNK cells and ILC1s from *Prdm1*$^{+/+}$ and *Prdm1* cko mice (n=5). (**J and K**) Proportion of GZMB$^+$ (**J**) and PRF1$^+$ (**K**) splenic NK cells at different maturation stages was analyzed by flow cytometry (n=5). Data are presented as the mean ± SEM and were analyzed by two-tailed, paired t-test. Differences were evaluated between littermates. Each circle and square on graphs represents an individual mouse; *P*, p-value; *, p<0.05; **, p<0.01, ns, not significant.

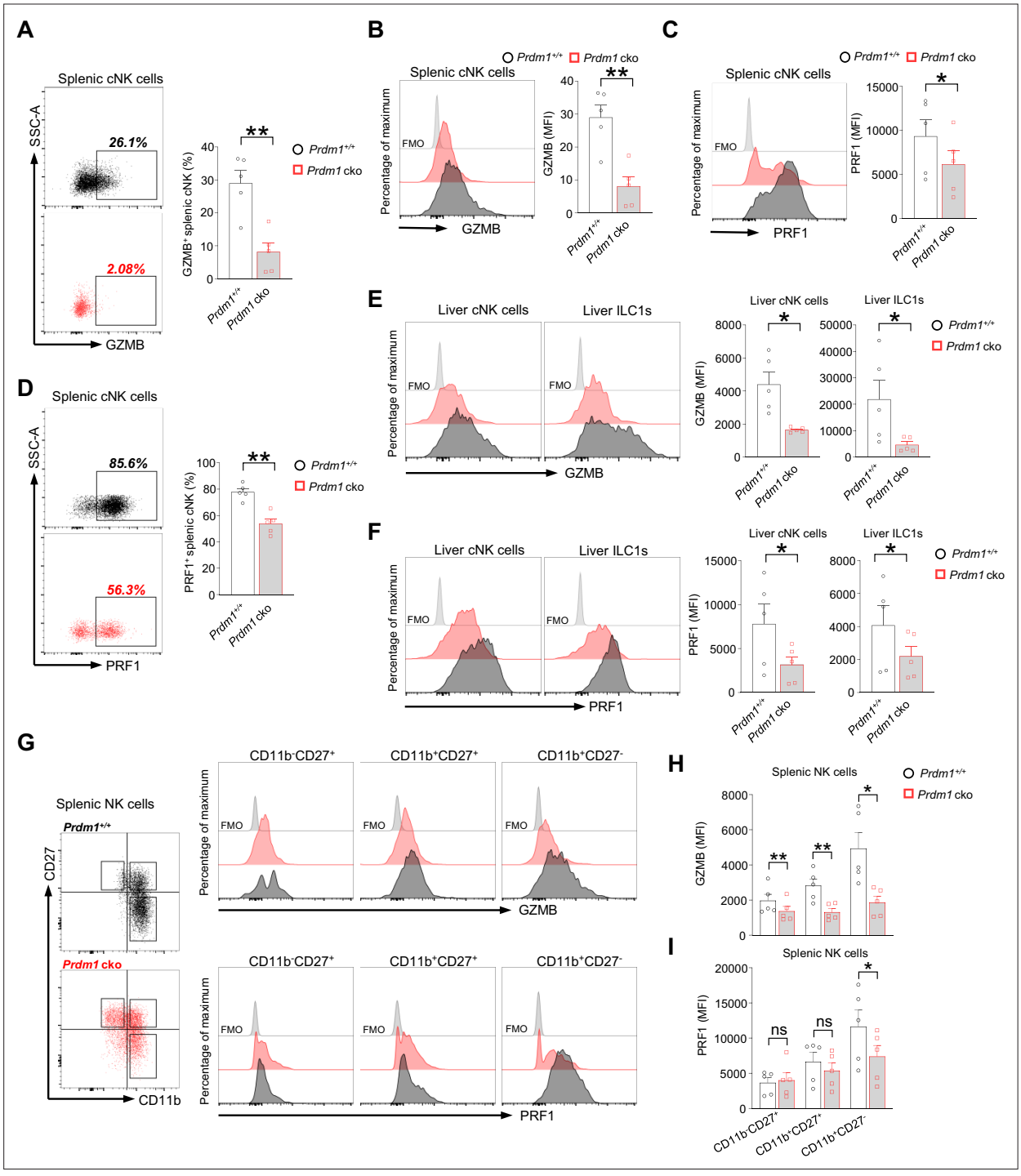

Figure 3—figure supplement 1. *Prdm1* deficiency impairs production of Granzyme B and Perforin in group 1 ILC. (**A–D**) Representative flow cytometric plot (left) and summary data (right) showing the proportion of GZMB$^+$ (**A**) and PRF1$^+$ (**D**) splenic cNK cells and relative mean fluorescence intensities (MFIs) of GZMB (**B**) and PRF1 (**C**) in splenic NK cells from *Prdm1*$^{+/+}$ and *Prdm1* cko mice (n=5). (**E and F**) Representative flow cytometric plots (left) and cumulative data (right) showing the relative MFIs of GZMB (**E**) and PRF1 (**F**) in liver cNK cells and ILC1s from *Prdm1*$^{+/+}$ and *Prdm1* cko mice (n=5). (**G–I**) Splenic NK cells were divided into different stages according to the expression of maturation markers CD11b and CD27. Representative flow cytometric plot (**G**) and showing the MFIs of GZMB (**H**) and PRF1 (**I**) in evaluated between littermates. Data are presented as the mean ± SEM and were analyzed by two-tailed, paired t-test. Differences were evaluated between littermates. Each circle and square on graphs represents an individual mouse; *P*, p-value; r, pearson correlation coefficient; *, p<0.05; **, p<0.01, ns, not significant.

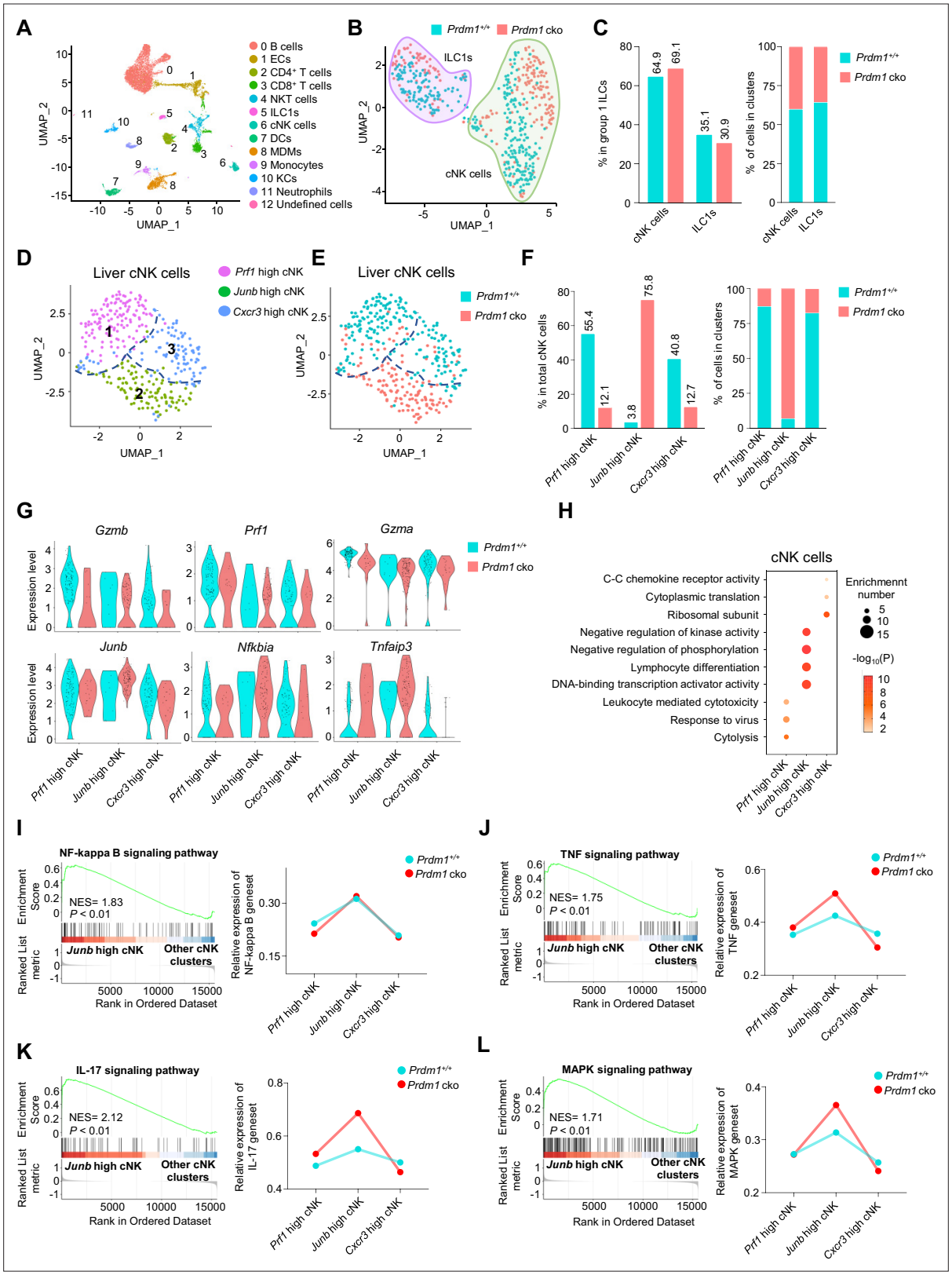

Figure 4. Different properties of cNK clusters following *Prdm1* knockout. (**A**) Uniform manifold approximation and projection (UMAP) visualization of liver CD45$^+$ cells from *Prdm1*$^{+/+}$ and *Prdm1* cko mice. Twelve clusters were defined and indicated by distinct colours. Each dot represents a single cell. (**B**) UMAP visualization of liver cNK and ILC1 clusters. Cells were colored by genotypes (*Prdm1*$^{+/+}$-blue; *Prdm1* cko-red). (**C**) Percentages of cNK cells and ILC1s in total group 1 ILCs (left), and their distribution in each cluster (right). (**D and E**) UMAP visualization of three different liver cNK clusters

Figure 4 continued on next page

Figure 4 continued

from two mouse strains. (**F**) Proportions of cNK cells among total cNK cells (left; 211 cells in *Prdm1*$^{+/+}$, and 141 cells in *Prdm1* cko) and within clusters (right). (**G**) Violin plots showing the normalized expression of select genes in different cNK clusters. (**H**) Enriched GO term of marker genes in three cNK clusters. Dot size represents enriched gene number, and color intensity represents significance. (**I–L**) GSEA plots (left) depicting the enrichment of NF-kappa B (**I**), TNF (**J**), IL-17 (**K**), and MAPK (**L**) signaling pathway in *Junb* high cNK cluster compared with clusters of *Prf1* high and *Cxcr3* high cNK cells. Right panel showed dynamic relative expression of the given gene sets from cluster1 to cluster3 between *Prdm1*$^{+/+}$ and *Prdm1* cko. Dots represent the average expression of given gene set in each cell, which was calculated through the sum of normalized expression of each individual gene within the designated gene set in every single cell. NES, normalized enrichment score.

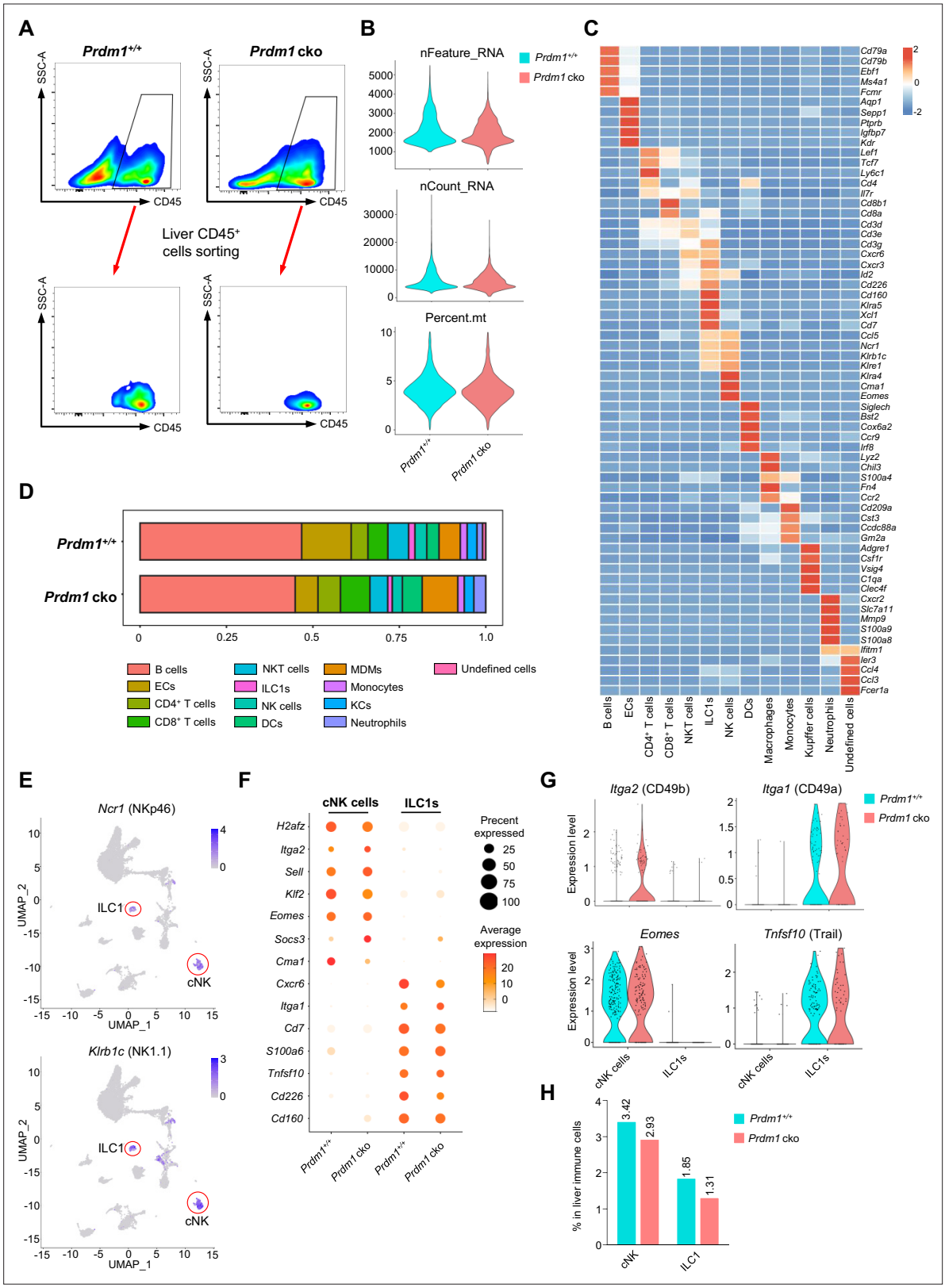

Figure 4—figure supplement 1. scRNA-seq identified subsets of liver CD45⁺ cell from *Prdm1*$^{+/+}$ and *Prdm1* cko mice. (**A**) Liver CD45⁺ cells from *Prdm1*$^{+/+}$ and *Prdm1* cko mice were FACS-sorted for scRNA-seq. (**B**) Quality control of the scRNA-seq data. Violin plot showing the nFeature_RNA, nCount_RNA, and percentage of mitochondrial genes of sequencing cells. nFeature_RNA represents the number of genes detected in each cell, and nCount_RNA represents the total number of molecules detected within a cell. (**C**) Heatmap showing the expression of top 5 upregulated DEGs of each

Figure 4—figure supplement 1 continued on next page

Figure 4—figure supplement 1 continued

cell cluster by log fold change (computed using Wilcox test in the 'FindAllMarkers' function of Seurat, avg_log2FC >0.25; p<0.05). (**D**) Population of twelve liver CD45^{+} cell clusters between *Prdm1*$^{+/+}$ and *Prdm1* cko mice. (**E**) Feature plots showing the normalized expression of *Ncr1* (NKp46) and *Klrbc1* (NK1.1) for different cell clusters. (**F**) Dot plot showing the normalized expression of marker genes in liver cNK cells and ILC1s clusters between *Prdm1*$^{+/+}$ and *Prdm1* cko. The dot size represents the percentage of cells expressing selected genes, and color intensity represents the average expression. (**G**) Violin plots showing the expression of marker genes *Itga2* (CD49b), *Itga1* (CD49a), *Eomes*, *and Tnfsf10* (Trail) between liver cNK cells and ILC1s between *Prdm1*$^{+/+}$ and *Prdm1* cko mice. (**H**) The percentage of liver cNK cells and ILC1s in liver immune cells between *Prdm1*$^{+/+}$ and *Prdm1* cko.

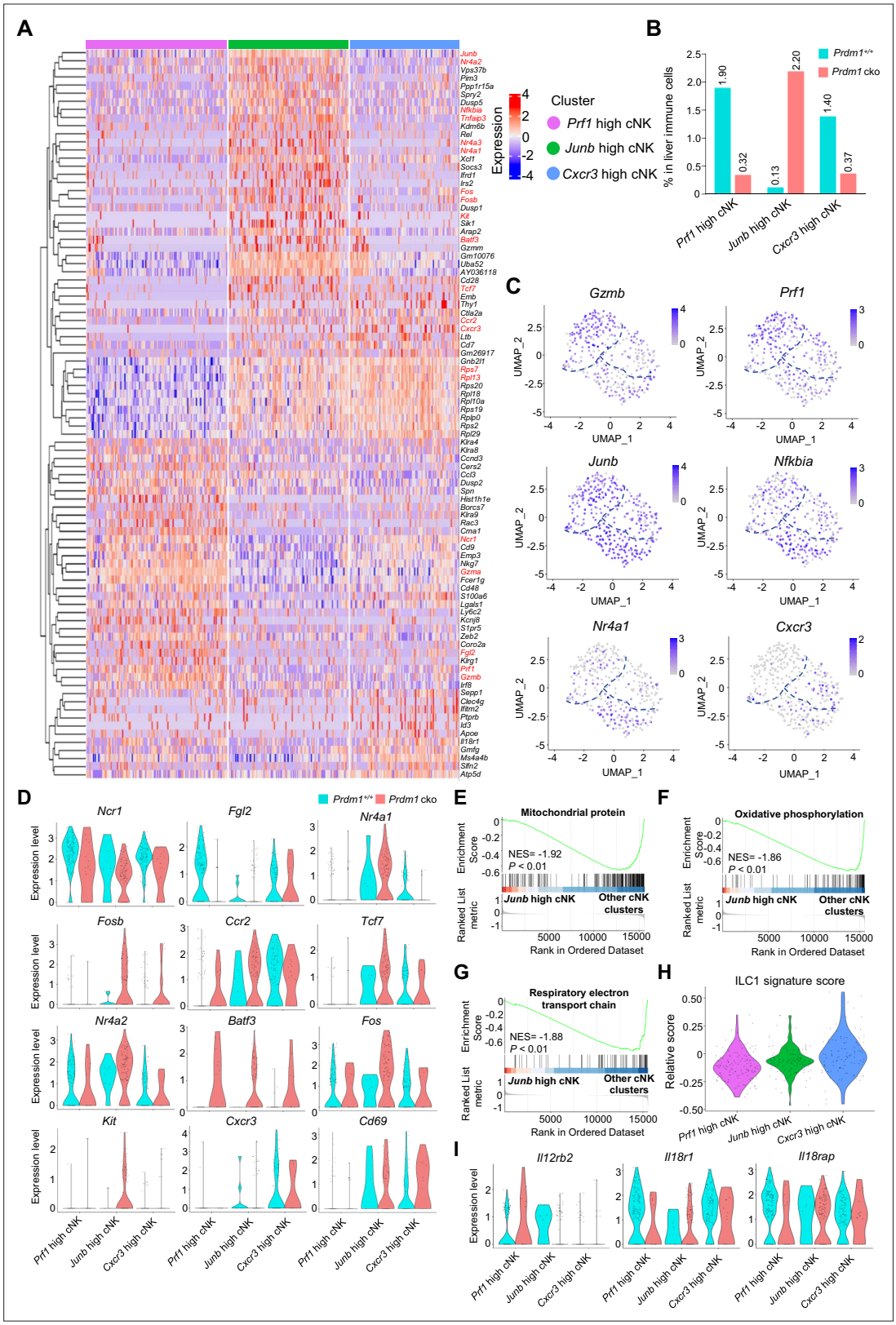

Figure 4—figure supplement 2. Cluster-specific markers of liver cNK cell clusters. (**A**) Heatmap showing the expression of top 30 upregulated DEGs by log fold change (computed using Wilcox test in the 'FindAllMarkers' function of Seurat, avg_log2FC >0.25; p<0.05), across the three liver cNK cell clusters (*Prf1* high cNK, *Junb* high cNK, *Cxcr3* high cNK) within *Prdm1*$^{+/+}$ and *Prdm1* cko mice. (**B**) The percentage of *Prf1* high cNK, *Junb* high cNK, and *Cxcr3* high cNK cells in liver immune cells between *Prdm1*$^{+/+}$ and *Prdm1* cko. (**C**) Feature plots showing the normalized expression of selected markers

Figure 4—figure supplement 2 continued on next page

Figure 4—figure supplement 2 continued

for liver cNK cell populations. (**D**) Violin plots showing the normalized expression of DEGs for each cNK cluster within *Prdm1*$^{+/+}$ and *Prdm1* cko mice. (**E–G**) GSEA of the enrichment of Mitochondrial protein (**E**), Oxidative phosphorylation (**F**), and Respiratory electron transport chain (**G**) in *Junb* high cNK cluster compared with clusters of *Prf1* high and *Cxcr3* high cNK cells. NES, normalized enrichment score. (**H**) Violin plot showing the ILC1 signature score for different cNK cell clusters, calculated using the signature genes of ILC1 cluster. (**I**) Violin plots showing the normalized expression of cytokine receptor genes (*Il12rb2*, *Il18r1*, and *Il18rap*) for each cNK cluster within *Prdm1*$^{+/+}$ and *Prdm1* cko mice.

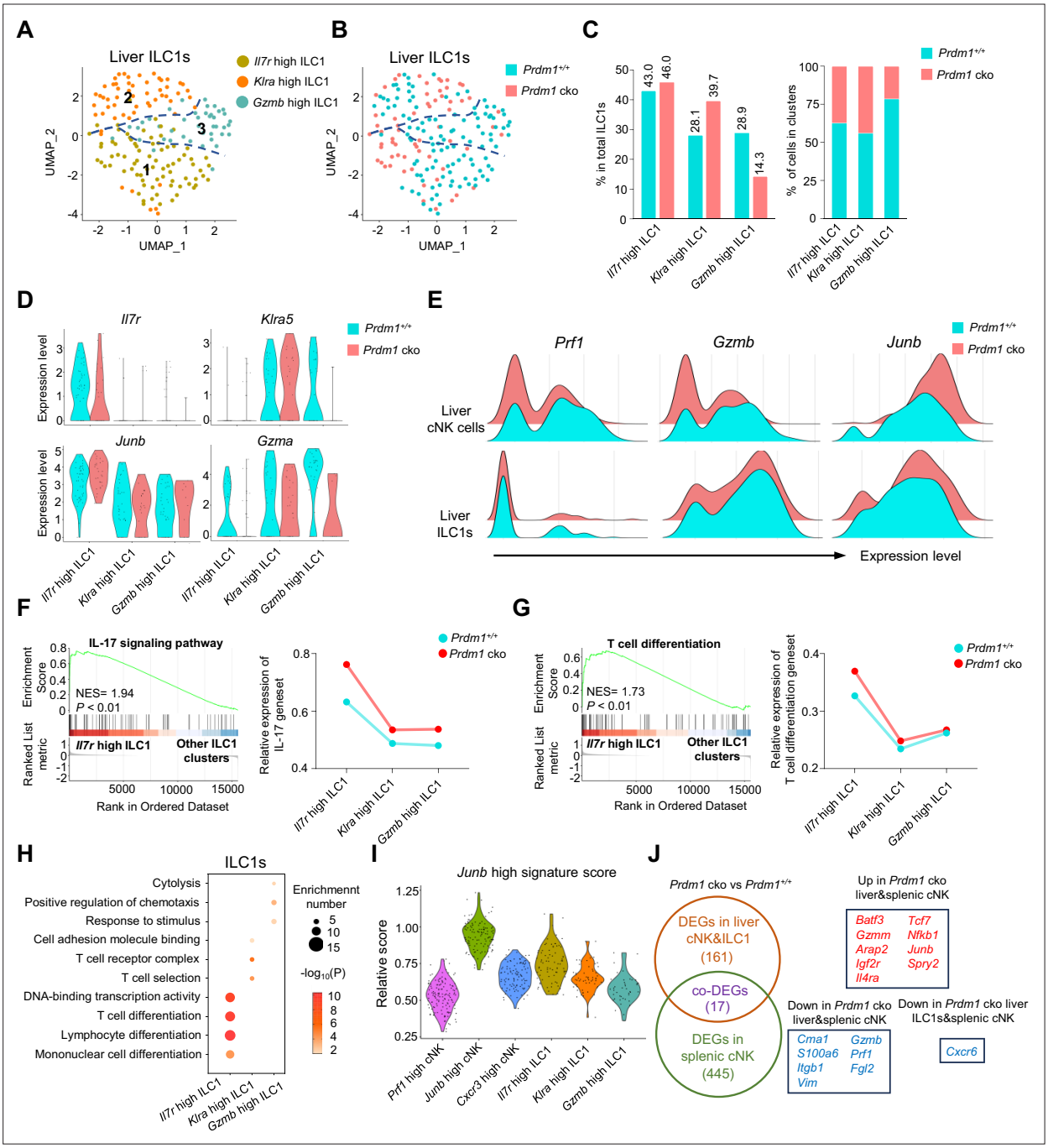

Figure 5. Different properties of ILC1 clusters following *Prdm1* knockout. (**A and B**) UMAP visualization of three different liver ILC1 clusters from two mouse strains. (**C**) Proportions of ILC1s among total ILC1s in different genotypes (left; 114 cells in *Prdm1*$^{+/+}$, and 63 cells in *Prdm1* cko) and within each cluster (right). (**D**) Violin plots showing the normalized expression of select genes in different ILC1 clusters. (**E**) Ridge plots showing the normalized expression of *Gzmb*, *Prf1*, and *Junb* in cNK and ILC1 clusters between *Prdm1*$^{+/+}$ and *Prdm1* cko cells. (**F and G**) GSEA plots (left) depicting the enrichment of IL-17 signaling pathway (**F**) and T cell differentiation (**G**) in *Il7r* high ILC1 cluster compared with clusters of *Klra* high and *Gzmb* high ILC1s. Right panel showed dynamic relative expression of the given gene sets from cluster1 to cluster3 between *Prdm1*$^{+/+}$ and *Prdm1* cko. Dots represent the average expression of given gene set in each cell, which was calculated through the sum of normalized expression of each individual gene within the designated gene set in every single cell. NES, normalized enrichment score. (**H**) Enriched GO term of marker genes in three ILC1 clusters. Dot size represents enriched gene number, and color intensity represents significance. (**I**) Violin plot showing the *Junb* high signature score for cNK cell and ILC1 clusters, calculated using the signature genes of *Junb* high cNK cluster. (**J**) Venn diagram showing overlapping and unique DEGs in comparisons within liver cNK cells, ILC1s and splenic cNK cells between *Prdm1*$^{+/+}$ and *Prdm1* cko(left), and 17 overlapped DEGs were shown at the right panel.

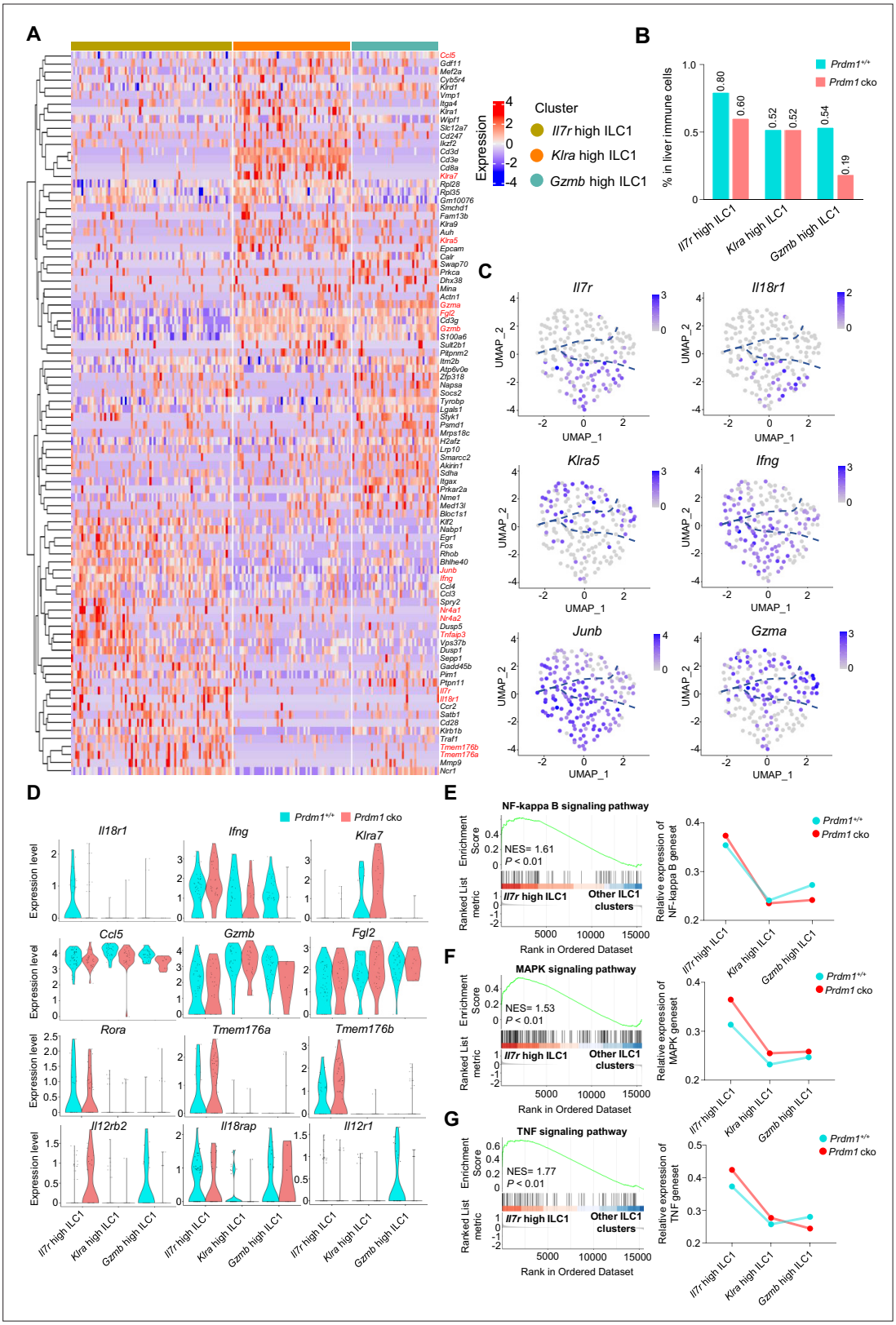

Figure 5—figure supplement 1. Cluster-specific markers of liver ILC1 clusters. (**A**) Heatmap showing the expression of top 30 upregulated DEGs by log fold change (computed using Wilcox test in the 'FindAllMarkers' function of Seurat, avg_log2FC >0.25; p<0.05), across the three ILC1 clusters (*Il7r* high ILC1, *Klra* high ILC1, *Gzma* high ILC1) within *Prdm1*$^{+/+}$ and *Prdm1* cko mice. (**B**) The percentage of *Il7r* high ILC1, *Klra* high ILC1, and *Gzma* high ILC1 in liver immune cells between *Prdm1*$^{+/+}$ and *Prdm1* cko. (**C**) Feature plots showing the normalized expression of selected markers for liver ILC1 populations.

Figure 5—figure supplement 1 continued on next page

Figure 5—figure supplement 1 continued

(**D**) Normalized expression of DEGs for each ILC1 cluster within *Prdm1*$^{+/+}$ and *Prdm1* cko mice. (**E–G**) GSEA plots (left) depicting the enrichment of NF-kappa B (**E**), MAPK (**F**), and TNF (**G**) signaling pathways in *Il7r* high ILC1 cluster compared with clusters of *Klra* high and *Gzma* high ILC1s. Right panel showed dynamic relative expression of the given gene sets from cluster1 to cluster3 between *Prdm1*$^{+/+}$ and *Prdm1* cko. Dots represent the average expression of given gene set in each cell, which was calculated through the sum of normalized expression of each individual gene within the designated gene set in every single cell. NES, normalized enrichment score.

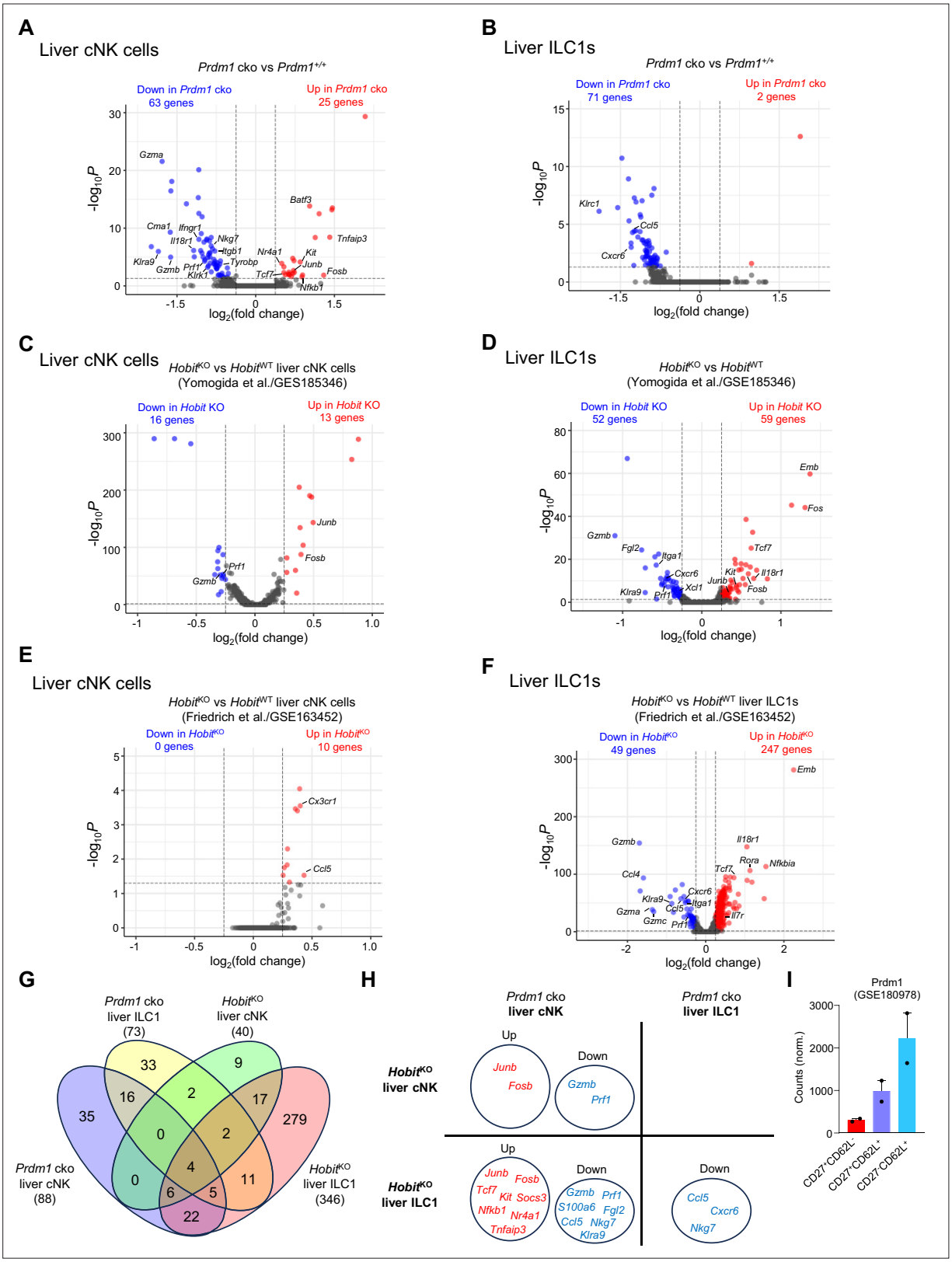

Figure 5—figure supplement 2. Similar and unique gene expression patterns in group 1 ILCs regulated by *Prdm1* and *Hobit*. (**A and B**) Volcano plots showing the DEGs (avg_log2FC >0.25; p<0.05) in *Prdm1* cko liver cNK cells (**A**) and ILC1s (**B**) compared to $Prdm1^{+/+}$ samples. (**C–F**) $Hobit^{KO}$ liver cNK cell and ILC1 clusters were identified from published scRNA-seq data (GES185346 and GSE163452). Volcano plots showing the DEGs (avg_log2FC >0.25; p<0.05) in $Hobit^{KO}$ liver cNK cells (**C and E**) and ILC1s (**D and F**) in comparisons within $Hobit^{WT}$ clusters. (**G**) Venn diagram showing the overlapped DEGs

Figure 5—figure supplement 2 continued on next page

Figure 5—figure supplement 2 continued

within liver cNK cells and in *Prdm1* cko and *Hobit*^{KO} compared to control samples. (**H**) Selected DEGs common regulated in *Prdm1* cko and *Hobit*^{KO} liver cNK cells or ILC1s. Upregulated genes (red) and downregulated genes (blue) were indicated. (**I**) Bar plot showing mRNA normalized counts of *Prdm1* in specific NK cell population based on the published bulk RNA-seq data (Flommersfeld et al., GSE180978).

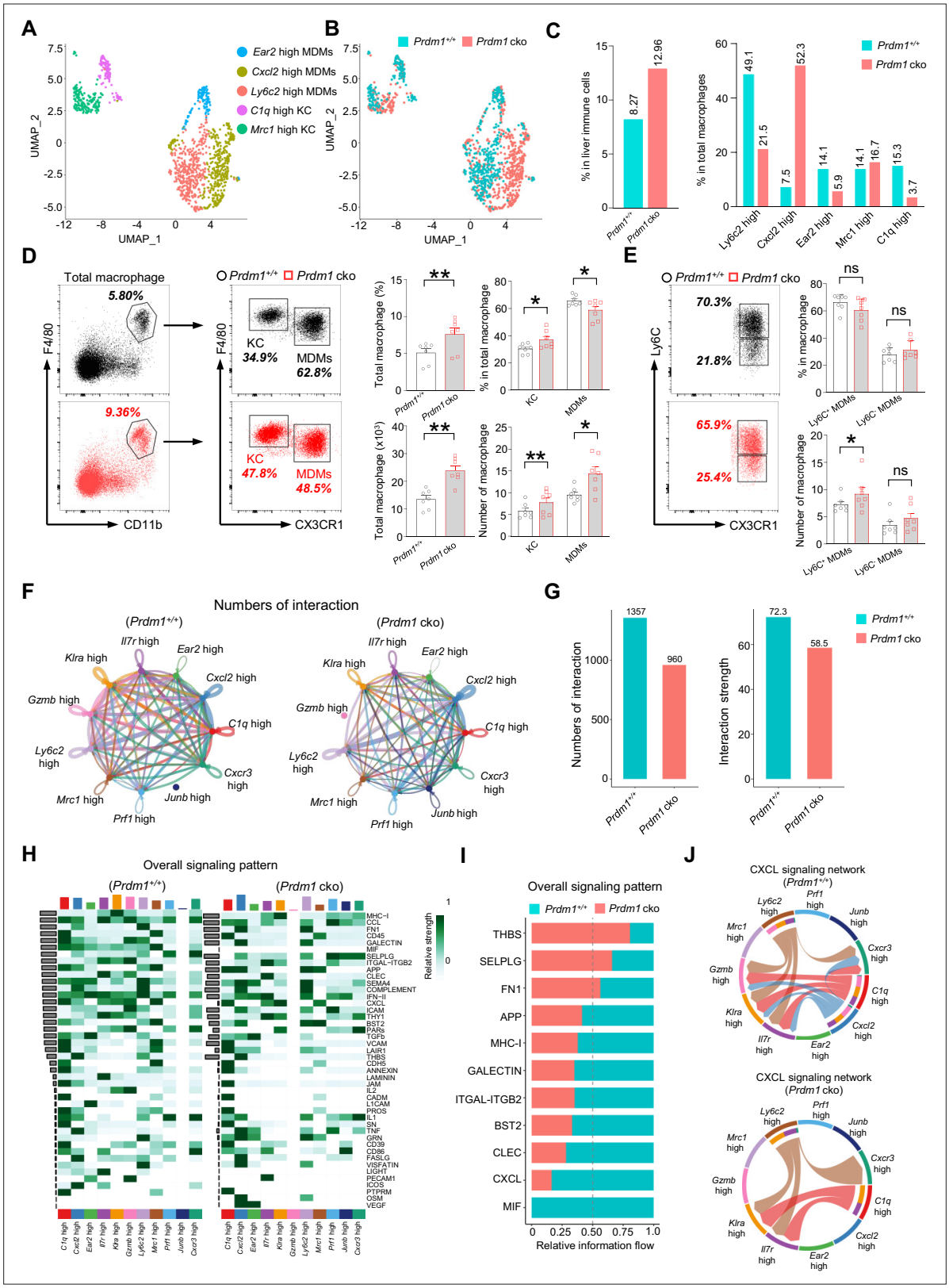

Figure 6. *Prdm1* facilitates the intercellular communication between liver group 1 ILCs and macrophages. (**A and B**) UMAP visualization of monocyte-derived macrophages (MDMs) and Kupffer cells (KCs) cluster (**A**) between *Prdm1*$^{+/+}$ and *Prdm1* cko (**B**). (**C**) Proportions of total macrophages in liver immune cells (left), and proportions of MDMs and KCs among total macrophages in different genotypes (510 cells in *Prdm1*$^{+/+}$, and 624 cells in *Prdm1* cko). (**D**) Representative flow cytometric plots (left) and cumulative data (right) of the percentage and absolute numbers of liver total macrophages

Figure 6 continued on next page

Figure 6 continued

(CD45$^+$Ly6G$^-$CD11b$^+$F4/80$^+$), MDMs (CX3CR1$^-$), and KCs (CX3CR1$^+$) between *Prdm1*$^{+/+}$ and *Prdm1* cko (n=7). (**E**) Representative flow cytometric plots (left) and cumulative data (right) of the percentage and absolute numbers of Ly6C$^-$ and Ly6C$^+$ cells in MDMs. (**F and G**) Circle plots (**F**) and summary data (**G**) illustrating the interaction numbers and strength of significant enriched ligand–receptor pairs among cluster of liver cNK cells, ILC1s, and macrophages from *Prdm1*$^{+/+}$ (left) and *Prdm1* cko (right) cells. The thickness of the line indicates the number of enrich pairs, and the arrow reflects the direction of the interaction. (**H**) Heatmap of overall signaling pattern recognized from ligand-receptor pairs, which contained the sum of signaling from the sender and target cells. (**I**) Bar graphs showing the information flow in selected active signaling patterns between *Prdm1*$^{+/+}$ and *Prdm1* cko cells. Relative information flow was calculated as the sum of the communication probability in given signaling patterns. (**J**) Chord plot of the CXCL signaling interaction network among cluster of liver cNK cells, ILC1s, and macrophages between *Prdm1*$^{+/+}$ and *Prdm1* cko cells. Data are presented as the mean ± SEM and were analyzed by two-tailed, paired t-test. Differences were evaluated between littermates. Each circle and square on graphs represents an individual mouse; *P*, p-value; *, p<0.05; **, p<0.01, ns, not significant.

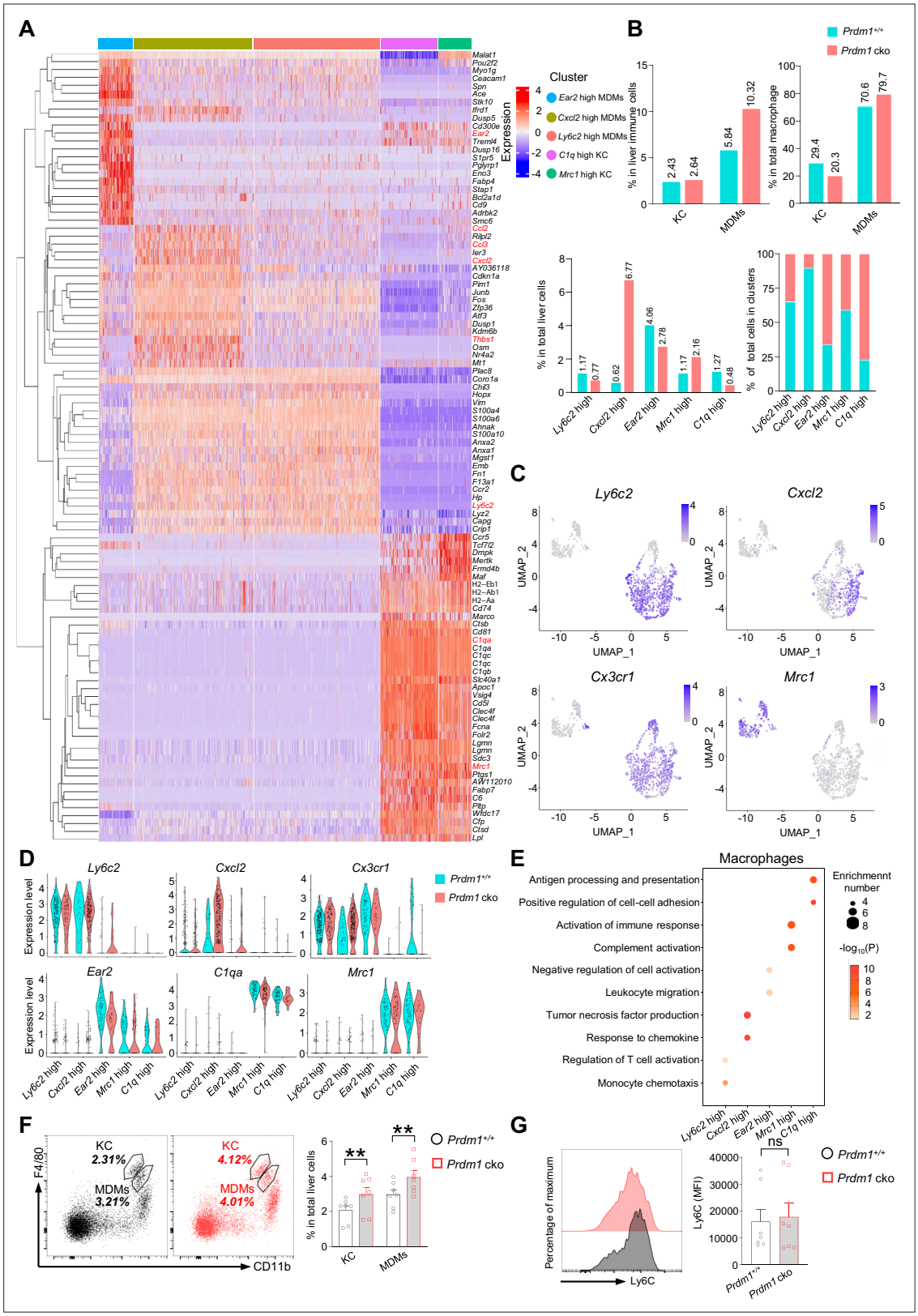

Figure 6—figure supplement 1. Identification of distinct macrophage clusters. (**A**) Heatmap showing the top 20 upregulated DEGs across four macrophage clusters (computed using Wilcox test in the 'FindAllMarkers' function of Seurat, avg_log2FC >0.25; *P*<0.05). (**B**) Proportions of macrophages (including monocyte-derived macrophages (MDMs) and Kupffer cells (KCs) cluster) in liver immune cells (top, left). Proportions of KCs and MDMs in total macrophages (top, right).The percentage of distinct macrophage clusters in liver total macrophages (bottom, left) and within

Figure 6—figure supplement 1 continued on next page

Figure 6—figure supplement 1 continued

clusters (bottom, right) between *Prdm1*$^{+/+}$ and *Prdm1* cko. (**C**) Feature plots showing the normalized expression of selected markers for macrophage populations. (**D**) Violin plots showing the expression of selected markers of each macrophage cluster within *Prdm1*$^{+/+}$ and *Prdm1* cko mice. (**E**) GO analysis of five distinct macrophage clusters. Dot size represents enriched gene number, and color intensity represents significance. (**F**) Representative flow cytometric plots (left) and cumulative data (right) showing the proportions of KCs and MDMs in total liver cells (**G**) Representative flow cytometric plots (left) and cumulative data (right) showing the relative MFIs of Ly6C in liver MDMs. Data are presented as the mean ± SEM and were analyzed by two-tailed, paired t-test. Differences were evaluated between littermates. Each circle and square on graphs represents an individual mouse; *P*, p-value; *, $p<0.05$; **, $p<0.01$, ns, not significant.

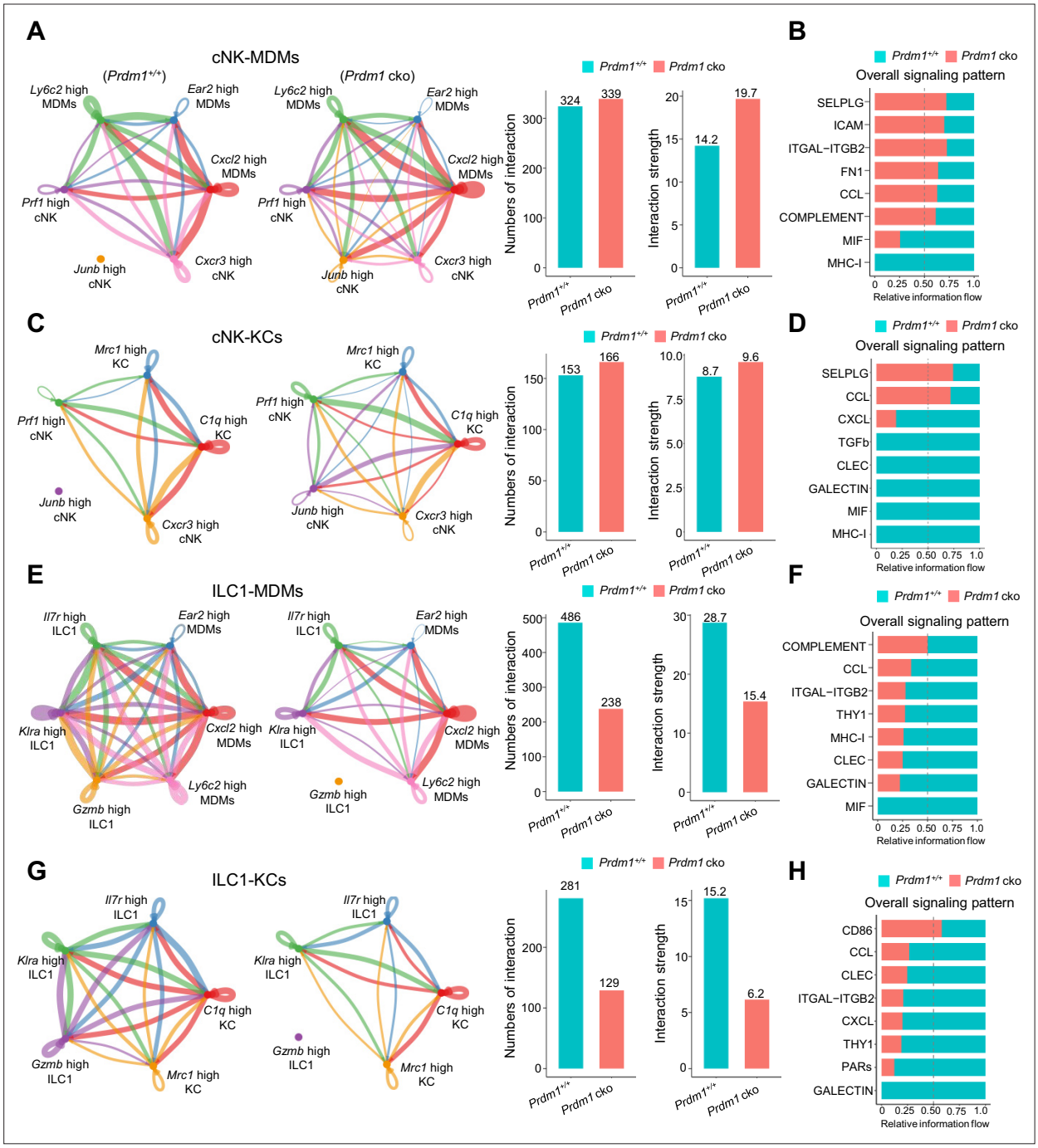

Figure 6—figure supplement 2. Cell-Cell communication between liver cNK, ILC1s, MDMs, and KCs. (**A, C, E and G**) Circle plots (left) and summary data (right) illustrating the interaction numbers and strength of significant enriched ligand–receptor pairs in cNK-MDMs (**A**), cNK-KCs (**C**), ILC1s-MDMs (**E**), ILC1-KCs (**G**) interactions between *Prdm1*$^{+/+}$ and *Prdm1* cko cells. The thickness of the line indicates the number of enrich pairs, and the arrow reflects the direction of the interaction. (B, D, F, and H) Bar graphs showing the information flow in selected active signaling patterns in cNK-MDMs (**B**), cNK-KCs (**D**), ILC1s-MDMs (**F**), ILC1-KCs (**H**) interactions between *Prdm1*$^{+/+}$ and *Prdm1* cko cells. Relative information flow was calculated as the sum of the communication probability in given signaling patterns.

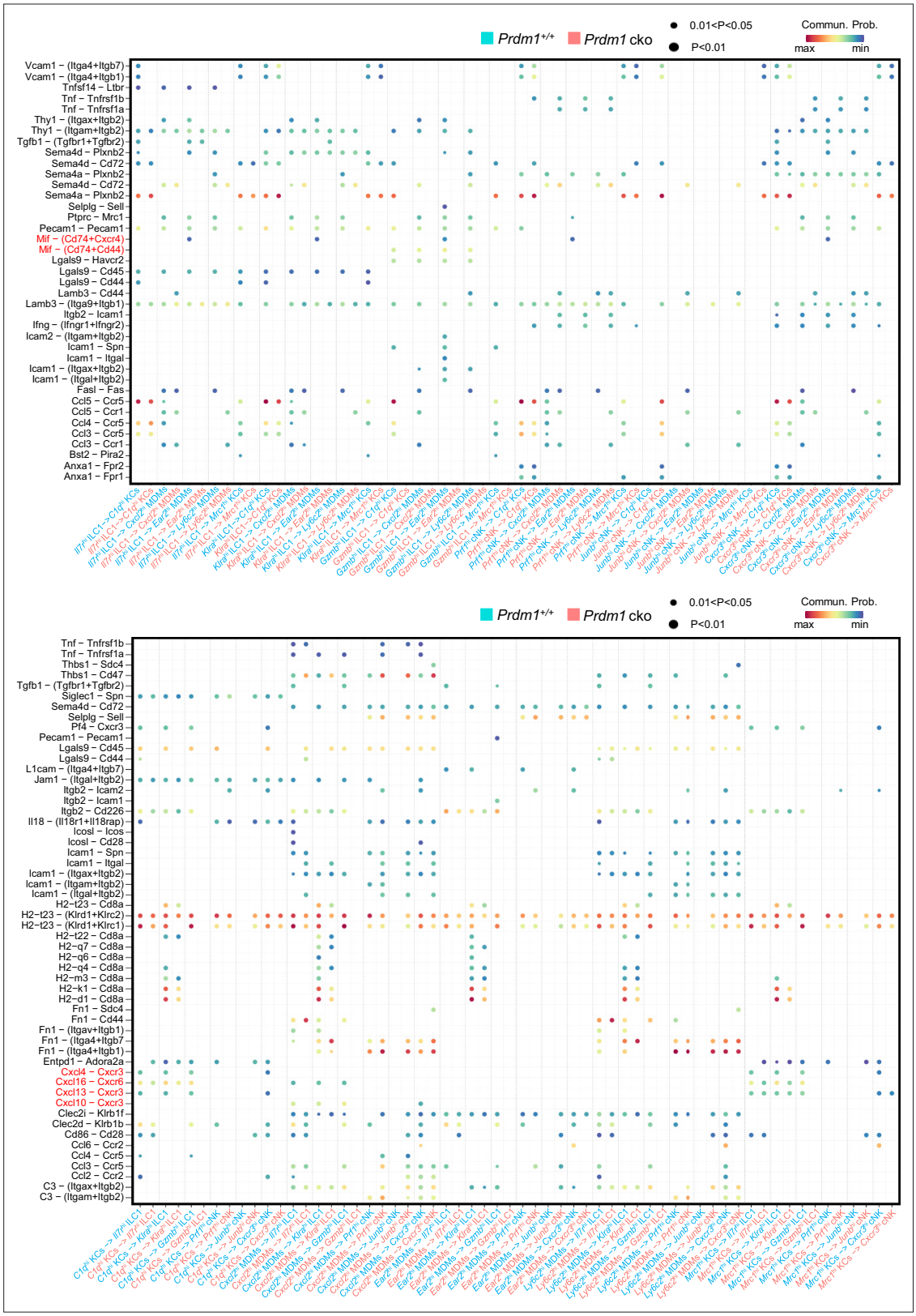

Figure 6—figure supplement 3. Ligand-receptor interaction between type I ILCs and macrophages. Bubble plots showing the significant ligand-receptor pairs between cNK cells, ILC1s, and macrophages within *Prdm1*$^{+/+}$ and *Prdm1* cko mice. The highlighted Mif-Cd74 and Cxcl-Cxcr signaling was significantly decreased in *Prdm1* cko mice. Dot size represents the *P*-value, and color intensity represents the communication probabilities. Empty space indicates a communication probability of zero. p-value were calculated by the one-sided permutation test.

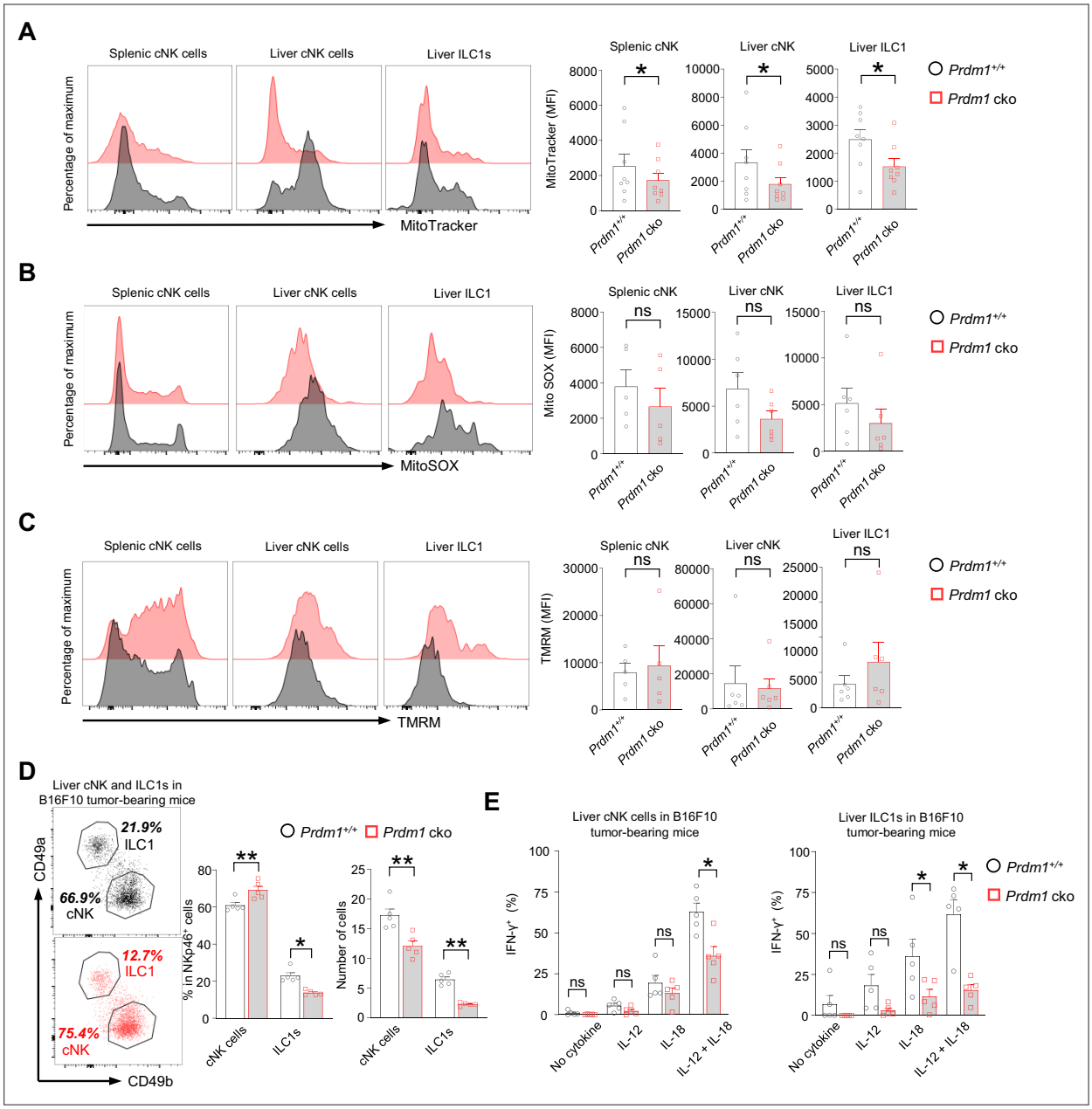

Figure 7. *Prdm1* safeguards group 1 ILCs from exhaustion-like phenotypes in the tumor microenvironment. (**A–C**) The Mitochondrial mass (MitoTracker Green staining; n=8) (**A**), Mitochondrial ROS (MitoSOX staining; n=5) (**B**), and Mitochondrial membrane potential (TMRM staining; n=5) (**C**) of splenic cNK cells, liver cNK cells and ILC1s were analyzed by flow cytometry. Representative flow cytometric plots (left) and cumulative data (right) showing the relative mean fluorescence intensities (MFIs) of each group. (**D**) Representative flow cytometric plots (left) and cumulative data (right) showing the percentage and absolute number of liver cNK cells and ILC1s in *Prdm1*$^{+/+}$ and *Prdm1* cko tumor-bearing mice at day 14 after inoculation with B16F10 melanoma cells via intrasplenic injection(n=5). (**E**) Percentages of IFN-γ^{+} liver cNK cells and ILC1s from *Prdm1*$^{+/+}$ and *Prdm1* cko tumor-bearing mice (n=5). Data are presented as the mean ± SEM and were analyzed by two-tailed, paired t-test. Differences were evaluated between littermates. Each circle and square on graphs represents an individual mouse; *P*, p-value; *, p<0.05; **, p<0.01, ns, not significant.

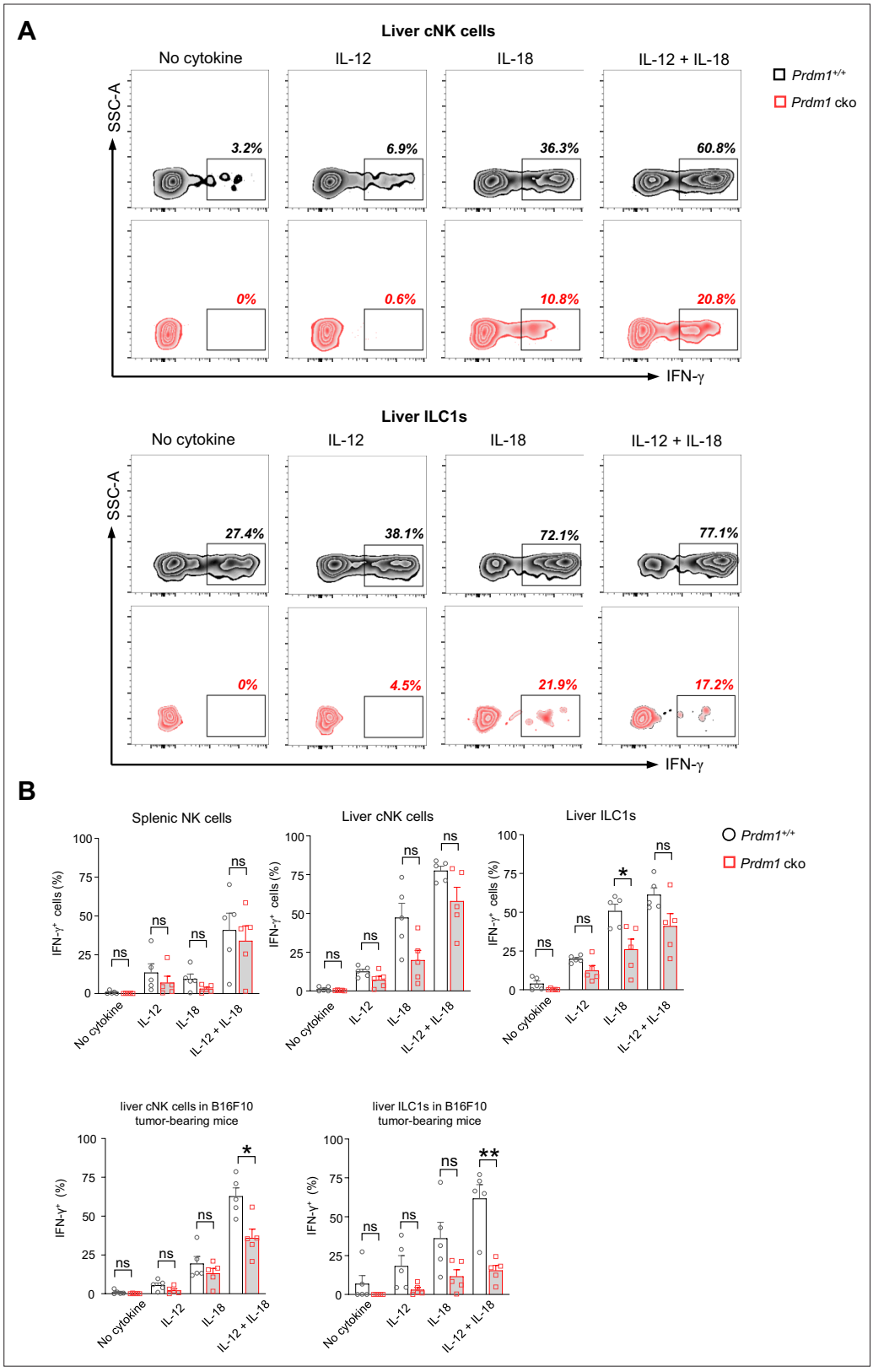

Figure 7—figure supplement 1. *Prdm1* maintains the IFN-γ production of liver type 1 ILCs in tumor microenvironment. (**A**) Representative flow cytometric plot of the frequency of IFN-γ$^+$ liver cNK cells and ILC1s from *Prdm1*$^{+/+}$ and *Prdm1* cko tumor-bearing mice at day 14 after inoculation with B16F10 melanoma cells via intrasplenic injection (n=5). (**B**) reanalysis of statistical significance of IFN-γ production in liver cNK cells and ILC1s

Figure 7—figure supplement 1 continued on next page

Figure 7—figure supplement 1 continued

after IL-12/IL-18 stimulation (***Figure 2F*** and ***Figure 7E***) using unpaired t-test. Data are presented as the mean ± SEM and were analyzed by two-tailed, paired or unpaired t-test. Differences were evaluated between littermates. Each circle and square on graphs represents an individual mouse; *P*, p-value; *, $p<0.05$; **, $p<0.01$, ns, not significant.